Analysis of the composition of the passive film on iron under pitting conditions in 0.05 M NaOH/NaCl using Raman microscopy *in situ* with anodic polarisation and MCR-ALS

M. K. Nieuwoudt,[a*] J. D. Comins[a] and I. Cukrowski[b]

[a] Materials Physics Research Institute and DST/NRF Centre of Excellence in Strong Materials, University of the Witwatersrand, Johannesburg, Wits 2050, South Africa

[b] Department of Chemistry, University of Pretoria, Pretoria 0002, South Africa

*Correspondence to: M. K. Nieuwoudt, Materials Physics Research Institute and DST/NRF Centre of Excellence in Strong Materials, University of the Witwatersrand, Johannesburg, Wits 2050, South Africa. E-mail: m.nieuwoudt@auckland.ac.nz

Abstract

The composition of the surface film formed on pure iron was investigated in a solution of 0.05 M NaOH and 0.05 M NaCl. Raman spectra of the film were recorded *in situ* during anodic polarisation over the passive region after addition of the NaCl to the electrolyte, under conditions of preresonance enhancement using excitation at 636.4 nm. Multivariate curve resolution with alternating least squares analysis was applied to the spectra to measure the relative amounts of different iron oxide and oxyhydroxides in the film at different potentials. The water content was also determined in this way from Raman spectra recorded using excitation at 514.5 nm. It was found that the composition of the film and the amount of incorporated water were influenced by the applied anodic potential. The results show that stable pitting can occur when the composition changes from the primary constituents β-FeOOH and Green Complex (a hydrated, amorphous magnetite) with smaller amounts of γ-Fe_2O_3 and γ-FeOOH, to δ-FeOOH and Green Complex, simultaneously with a reduction in water content. These changes result in conditions that favour the rate of localised breakdown of the film by Cl^- ions over the rate of repassivation by water in the passive film.

Introduction

The passive film formed on iron and its localised breakdown in the presence of chloride ions has been extensively studied under a variety of different conditions, the associated literature being reviewed by a number of authors.[1-4] These studies have shown that the initiation and stability of localised breakdown of the passive film is affected by numerous factors. These include the condition of the iron surface, such as its surface roughness and the presence of defects, and the electrochemical environment comprising variables such as the electrolyte pH, the availability of dissolved oxygen, the temperature and the aggressive anion concentration.

The complexity in experimental conditions is the probable source of the different and sometimes conflicting mechanisms proposed for the initiation and growth of pits. However, there is general agreement on the pitting process in several respects, namely that: (1) localised adsorption of aggressive anions on the surface is the first step in pitting; (2)

adsorption of anions always occurs at defect sites on the surface; (3) a dynamic equilibrium exists between localised breakdown and repassivation of the passive film; and (4) when a critical level of aggressive anion concentration is reached at which repassivation is hindered, the equilibrium is shifted in favour of the localised breakdown and stable pitting occurs. The major difference in the mechanisms of the stable pitting proposed by the various pitting theories concerns whether the aggressive anion is incorporated into the passive film or not.[4]

Different models have been proposed[4] for the mechanism of pit formation in passive films on iron under the influence of chloride ions, the leading ones being: (1) the ion exchange model, in which Cl^- ions enter the film via cation vacancies or by ion exchange of Cl^- ions for O^{2-} ions; (2) the point defect model, in which cation diffusion occurs from the metal/film to the film/solution interface, resulting in formation of metal vacancies at the metal/film interface; when this occurs at a sufficiently high rate, voids form which grow and lead to local collapse of the passive film, resulting in faster dissolution than the rest of the film and growth of pits; (3) the adsorption-displacement models, in which breakdown results from dissolution of iron chloride complexes formed from simultaneous adsorption of Cl^- ions and displacement of oxygen from the monolayer said to constitute the passive layer; (4) the chemico-mechanical models, in which Cl^-ions adsorbed on the passive film reduce the interfacial tension at the film/solution interface, resulting in the formation of cracks or flaws from electrostriction pressure effects arising from repulsive forces between the adsorbed Cl^- ions; (5) the pore models, in which Cl^- ions pass through a porous passive film and form complexes with iron at the metal/film interface, which then diffuse outward through pores to the film/solution interface, resulting in pits at the bottom of the pores; and (6) the hydrated polymeric oxide model, in which Cl^- ions are adsorbed onto the layer and displace the bound water molecules, then form chloride-containing iron complexes that diffuse into the bulk solution to form soluble complexes.

Numerous studies of both iron and stainless steels in aqueous solutions of pH 8–14 have confirmed an increased water concentration in the surface film in the passive region[4-14] that grows with increasing pH.[4, 7] However, there are differences of opinion concerning the role of the incorporated water in the protective properties of the film. From an ellipsometric study[9] of iron in 0.05 M NaOH with added chloride, it was suggested that the incorporated water contributed to pitting by facilitating the migration of chloride via water paths in the film. It was concluded that the passive film was composed of FeOOH incorporating a large amount of water, which decreased continuously as the passivation progresses, and that the film resisted pitting at a point in the formation of the film when the water content was sufficiently reduced. In other studies, the passive film has been described as a hydrated oxide with a gel-like structure[16] in which the bound water plays a critical role in assisting the repassivation of the film in the presence of chloride. X-ray photoelectron spectroscopy (XPS), secondary ion mass spectrometry and ion scattering spectroscopy studies[5] found that dehydration by heating resulted in chloride penetrating the whole film thickness. It was proposed that water transforms the properties of the iron oxide to those of the protective passive layer by keeping the film amorphous, which prevents Fe^{2+} ions from diffusing from the metal base to hydration sites at the oxide/solution interface. The XPS studies also showed that Cl^- ions can remove water in a process of depassivation. From *in situ* ellipsometric measurements of the passive film on Fe in 0.05 M NaOH with added

chloride,[15] microstructural changes were observed to occur within the anodic passive region just before and in the neighbourhood of the pitting potential, but the mechanism has not been established.

It has generally been agreed that the passive film consists basically of two layers. There is an inner, adherent and coherent layer with a spinel structure, consisting of Fe_3O_4, γ-Fe_2O_3 or an intermediate composite of Fe_3O_4/γ-Fe_2O_3[19-21] Various proposals have been made for the composition and structure of the outer layer in the passive region, namely $Fe(OH)_2$,[17, 22] a hydrated FeOOH (α-, β-, δ- and γ-forms),[9, 21] γ-FeOOH,[12, 23] a hydrated amorphous or polymeric oxide.[5, 11, 12, 24-26] In a recent study of the growth of the passive film on iron in 0.05 M NaOH using Raman microscopy *in situ* with preresonance enhancement during successive cycles of anodic and cathodic polarisation,[27] the iron oxides and oxyhydroxides present on the surface in the passive region were determined to be largely γ-Fe_2O_3, α-FeOOH, δ-FeOOH, γ-FeOOH and $Fe(OH)_2$. The relative amounts of these compounds were found to vary with potential within the passive region and also with different cycles. In addition, the amount of water was found to increase as the potential was increased into the passive region, but at higher anodic potentials the water content was found to decrease.

As discussed above, the presence of chloride ions induces pitting of iron in 0.05 M NaOH. Their presence also results in the formation of a dark green gelatinous precipitate. This has been referred to as Green Rust I [22, 28, 29] from the solid state oxidation of $Fe(OH)_2$. [29] This compound is considered to consist of positively charged brucite-like layers separated by interlayers of anions and water molecules. It belongs to the hydro-talcite mineral group, [24] whose composition has been described as $[Fe^{II}_2Fe^{III}O_x(OH)_y]Cl_{(7-2x-y)}$, [30] $Fe^{III}_2Fe^{II}_4(OH)_{12}Cl_2$ [31] or varying between $Fe^{II}_3Fe^{III}(OH)_8Cl{\cdot}nH_2O$ and $Fe^{II}_{2.2}Fe^{III}(OH)_{6.4}Cl{\cdot}nH_2O$ with *n* probably equal to 2. [32] The Fe^{III}/Fe^{II} ratio increases continuously upon aerial oxidation and converts in air to Fe_3O_4 for slow oxidation, [22, 28] or to γ-FeOOH in the case of rapid oxidation. [22, 31, 33] Green Rust I includes amorphous iron oxyhydroxide ($FeO_2(OH)_{3-2x}$) as an intermediate which oxidises to α-FeOOH in strongly alkaline solutions. [22] From a Mössbauer study [34] it was found that different ferrous hydroxide compounds are involved in the formation of Green Rust I depending on the ratio of $[Cl^-]/[OH^-]$. For $[Cl^-]/[OH^-] \leq 1$, ferrous hydroxide I ($Fe(OH)_2$) forms which transforms into α-FeOOH and Fe_3O_4. For $[Cl^-]/[OH^-] \geq 1$, ferrous hydroxide II ($2Fe(OH)_2$,FeOHCl) forms, which transforms to Green Rust I, which in turn transforms into γ-FeOOH, with parallel formation of α-FeOOH and Fe_3O_4. For $[Cl^-]/[OH^-] \geq 4$, β-FeOOH is predominantly formed. In a separate XRD study [35] it was found that for $[Cl^-]/[OH^-] > 1.75$, γ-FeOOH, α-FeOOH and β-FeOOH were formed, and for $[Cl^-]/[OH^-]$ between 1.025 and 1.11 a hydrated magnetite of the form $Fe(OH)_2{\cdot}2FeOOH$ forms, which leads to a nonstoichiometric magnetite, $Fe_{3-x}O_4$. For $[Cl^-]/[OH^-]$ between 1 and 1.205 it was found that formation of hydrated magnetite occurred from hydrated ferrous hydroxide without formation of Green Rust I. [35] Because the $[Cl^-]/[OH^-]$ ratio in the electrolyte in the present study is unity, the compound formed after the addition of chloride could be either Green Rust I or a hydrated magnetite and thus the nomenclature Green Complex will be used for its description.

It was the purpose of the present work to further examine the state of the passive film in the presence of chloride by first investigating the relative amounts of the Green Complex and the seven iron oxide and oxyhydroxide compounds investigated previously [27] and

second by determining the relative amount of water incorporated in the film before and during the onset of stable pitting. Raman microscopy was performed *in situ* during anodic polarisation of the surface after addition of NaCl to create an electrolyte of 0.05 M NaOH and 0.05 M NaCl at the beginning of the passive region. This has provided new insights into the pitting process.

Experimental

Potentiodynamic polarisation

A 2-mm-thick disc was cut from a 10-mm-diameter rod of iron (99.8% pure single-crystal iron) using a diamond rotary blade. It was then polished with 1200 grit SiC and washed with distilled water and acetone. The disc was encased in epoxy with only the polished surface exposed and positioned 3 mm below the quartz window of a three-electrode cell, specially designed to fit on the stage of an Olympus confocal microscope attachment of a Jobin-Yvon T64000 Raman spectrograph. The cell design permitted the electrolyte to flow over the sample surface and to be circulated by means of a peristaltic pump. This prevented laser-induced heating of the sample. The electrolyte was not deaerated. A Metrohm Ag/AgCl reference electrode with 3.5 M KCl was used, connected by a Luggin probe of 0.5 mm inner diameter, positioned 2 mm from the iron surface. All potentials referred to are relative to this electrode, which is +0.196 V relative to the standard hydrogen electrode. The counter electrode was a Pt ring disc of thickness 0.2 mm, outer diameter 10 mm and was positioned 2 mm above the iron surface. The three electrodes were connected to a Schlumberger SI1286 potentiostat.

In the interest of clarity regarding the experimental approach and results, we provide a brief description of the phenomena taking place. These are discussed in more detail in [27] in the case of iron in 0.05 M NaOH. An iron surface which is subjected to anodic potentiodynamic polarisation in 0.05 M NaOH undergoes a series of oxidation reactions which eventually result in the formation of a stable passive film. The oxidation reactions give rise to current peaks over an active potential region and the onset of passivity is indicated by a drop in current density to negligible values over a passive potential region. When the surface is similarly polarised in the presence of chloride ions, breakdown of the passive film occurs at a specific potential in the passive region (the pitting potential, E_p), which is indicated by a sharp rise in current in the passive region.

In the present work, the iron surface was initially subjected to cathodic polarisation for 20 min at −1.40 V to remove oxide compounds formed in air and upon immersion in the 0.05 M NaOH solution. The surface was then subjected to anodic potentiodynamic polarisation in this solution resulting in oxidation reactions leading to a series of current peaks as shown in Fig. S1. The surface passivates from around −0.55 V in which the current initially falls and remains at a very low value until it rises again near 0.6 V because of the oxidation of water to O_2.

A passive film was grown on the surface by subjecting the iron to two cycles of potentiodynamic polarisation; for each cycle the potential was swept first anodically and then cathodically between −1.20 V and +0.60 V at a sweep rate of 10 mV/s, these

procedures being similar to those described previously. [27] During the third anodic sweep the potential was held at −0.55 V, being the beginning of the passive region as discussed above. At this point a solution of NaCl was added to the electrolyte such that its concentration in the electrolyte was 0.05 M, so that the resulting electrolyte solution was 0.05 M NaOH + 0.05 M NaCl with pH 12.7. The potential was kept at −0.55 V and the current was then monitored as a function of time for 1200 s. During this period, Raman spectra were recorded of the iron surface as discussed below. The potential was then increased by +0.10 V and held there for another 1200 s while corresponding current and Raman measurements were carried out. This procedure was repeated until the pitting potential was reached, being that at which stable pitting occurred as indicated by a steady sharp increase in current. At this point the potential was held constant while spectra were recorded of various pits that were visible and the surface regions adjacent to the respective pits. The potential was then increased above the pitting potential and spectra were again recorded of various pits and their adjacent surfaces.

The above experiment was repeated under identical conditions but using argon ion laser excitation of wavelength 514.5 nm after cleaning and polishing the iron sample to the same surface roughness. Thus, *in situ* Raman spectra could be recorded of the O–H stretch region at the same potentials as used previously.

Raman microscopy

A Jobin-Yvon T64000 Raman spectrograph fitted with a liquid nitrogen-cooled charge-coupled device detector was used in the single spectrograph mode with a holographic dispersive grating of 600 g/mm and a slit width of 200 µm giving a resolution of 6 cm^{-1}. The experimental conditions used for the Raman spectroscopy and the precautions taken were described in detail previously [27] and only a brief account is given here. The optimised excitation wavelength of 636.4 nm was obtained from a Spectra-Physics 375 tunable dye laser pumped by a Spectra-Physics 171 argon ion laser; the output beam power of the dye laser was 100–105 mW while the power at the quartz window of the electrochemical cell was 2 mW. The laser beam was focussed onto the iron surface with a spot size of diameter 5 µm. Raman spectra were recorded of the passive film *in situ* while the potential was increased. The spectral integration time was 130 s and two spectra were averaged for each measurement.

For the Raman spectra obtained *in situ* of the O–H stretch vibration between 4300 and 2300 cm^{-1}, the 514.5 nm excitation line of a Coherent Innova 308 argon-ion laser was used at an output power of 500 mW with 120 s integration time. This excitation wavelength was found to afford better intensities for the O–H stretch modes than 636.4 nm excitation. The other experimental conditions are identical to those described previously. [27]

Preparation of Green Complex for the MCR-ALS optimisation

The structure of synthetically prepared Green Rusts has often been found to differ from that of the Green Rusts in the corrosion products. [37, 38] For this study a Green Complex was prepared using reagents of the same chloride ion concentrations as those used in the electrolyte under pitting conditions. A 0.05 M $FeCl_2$ solution (10 ml) was added to 20 ml of a

0.05 M NaOH solution. A green gelatinous precipitate formed, which was quickly filtered, placed on a glass slide and covered with a cover slip to prevent rapid aerial oxidation. A Raman spectrum was immediately recorded of the prepared compound using 636.4 nm excitation line at a laser power of 19 mW (0.3 mW at the sample) and integration time of 130 s. Weak and broad bands were observed in the Raman spectrum at 555 cm^{-1} and 1097 cm^{-1}; with time the compound eventually converted to Fe_3O_4 (Fig. 1). The bands at 550 and 1097 cm^{-1} have been attributed to $Fe(OH)_2$. [23, 39] Green Rust I has been reported to have bands at 430, 503 cm^{-1} [22] or 505 cm^{-1} [31] and 560 or 544 cm^{-1} because of the $Fe(OH)_2$ component, and at 303, 387 and 698 cm^{-1} from the $Fe(OH)_3$ component. [22] The compound formed therefore appears to be more a hydrated, amorphous magnetite compound than a Green Rust, and hence the nomenclature Green Complex will be used as discussed previously. This complex is considered to be more likely to form than Green Rust I in a solution of 0.05 M NaCl + 0.05 M NaOH.

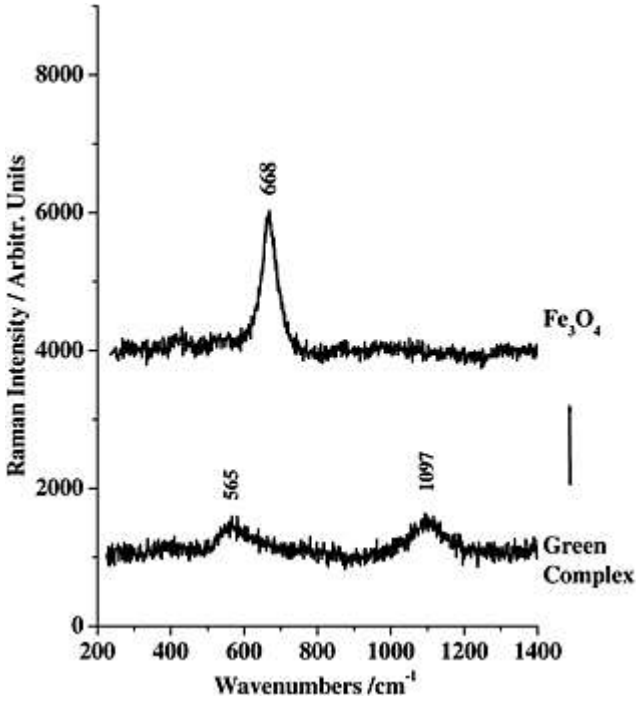

Figure 1. Raman spectra of freshly prepared Green Complex (lower spectrum), which converted with time to Fe_3O_4 (upper spectrum). The spectrum of Green Complex was truncated from 270 to 950 cm^{-1} for the MCR-ALS analysis. The excitation wavelength was 636.4 nm.

Multivariate curve resolution with alternating least squares

A detailed description of this technique is provided in [27], being based on the Multivariate curve resolution with alternating least squares (MCR-ALS) toolbox of MATLAB. [40] It is a least squares optimisation method that enables a determination of the relative amounts of components present in a mixture by performing iterative optimisation of the resolved concentration and spectral profiles of the individual components subject to selected constraints. The spectra of the seven individual pure iron oxide and oxyhydroxide compounds, recorded previously, [36] namely Fe_3O_4 (magnetite), α-Fe_2O_3(hematite), γ-Fe_2O_3 (maghemite), α-FeOOH (goethite), β-FeOOH (akaganeite), δ-FeOOH (feroxyhyte) and γ-FeOOH (lepidocrocite) together with the spectrum of Green Complex were used as pure

component spectra for the optimisation. All spectra were adjusted to the same height for the instrumental peak at 1562 cm^{-1} for the optimisation. [27]

As discussed in our previous study, [27] the selection of the seven iron oxide and oxyhydroxide compounds was directly guided by earlier investigations of the passive film on the surface of iron in alkaline solutions using Raman, XPS, Mössbauer, ellipsometry and secondary ion mass spectrometry studies and their respective conclusions identifying these compounds as constituents. The MCR-ALS analysis has the advantage that a significant percentage lack of fit indicates the presence of additional compounds besides those chosen as the pure components. These residual components can be determined and identified as shown in our previous work. [27]

Multivariate curve resolution with alternating least squares optimisation was also used to monitor changes in the amount of water in the film over the passive region from the Raman spectra recorded *in situ* of the O–H stretch region, after adjusting the spectra to the same height for the instrumental peaks present in each spectrum at 2633 and 2669 cm^{-1}. [27]

Results

Raman spectra of the passive film at different potentials

After the addition of the 0.05 M sodium chloride at the beginning of the passive region, Raman spectra were recorded of the surface at various constant values of the applied potential between −0.55 V and +0.30 V for 1200 s using an excitation wavelength of 636.4 nm and a laser beam spot size of 5 µm diameter – the chronoamperometric data are shown in Fig. 2. At +0.10 V a sharp increase in current is observed after 1000 s, which signals the onset of stable pitting.

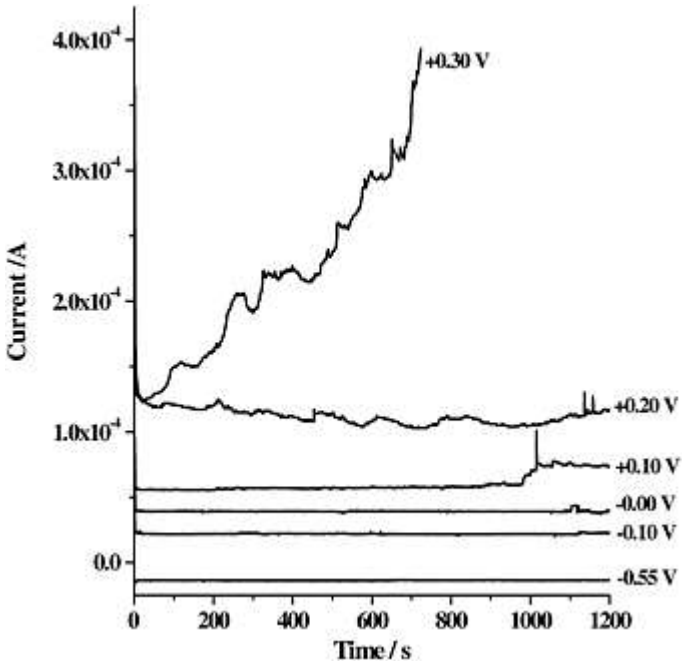

Figure 2. Chronoamperometric traces recorded at −0.55 V at 10 mV/s between −1.20 V and +0.60 V during the third potentiodynamic polarisation cycle after addition of 0.05 M NaCl to the 0.05 M NaOH solution.

The Raman spectra recorded at each applied potential are given in Fig. 3. The spectra have been corrected by the subtraction of a curved baseline, which increased continuously, particularly toward low wavenumber shifts arising from reflection by the metal surface and from the holographic notch filter used. [27] A polynomial fitting function was used in this procedure.

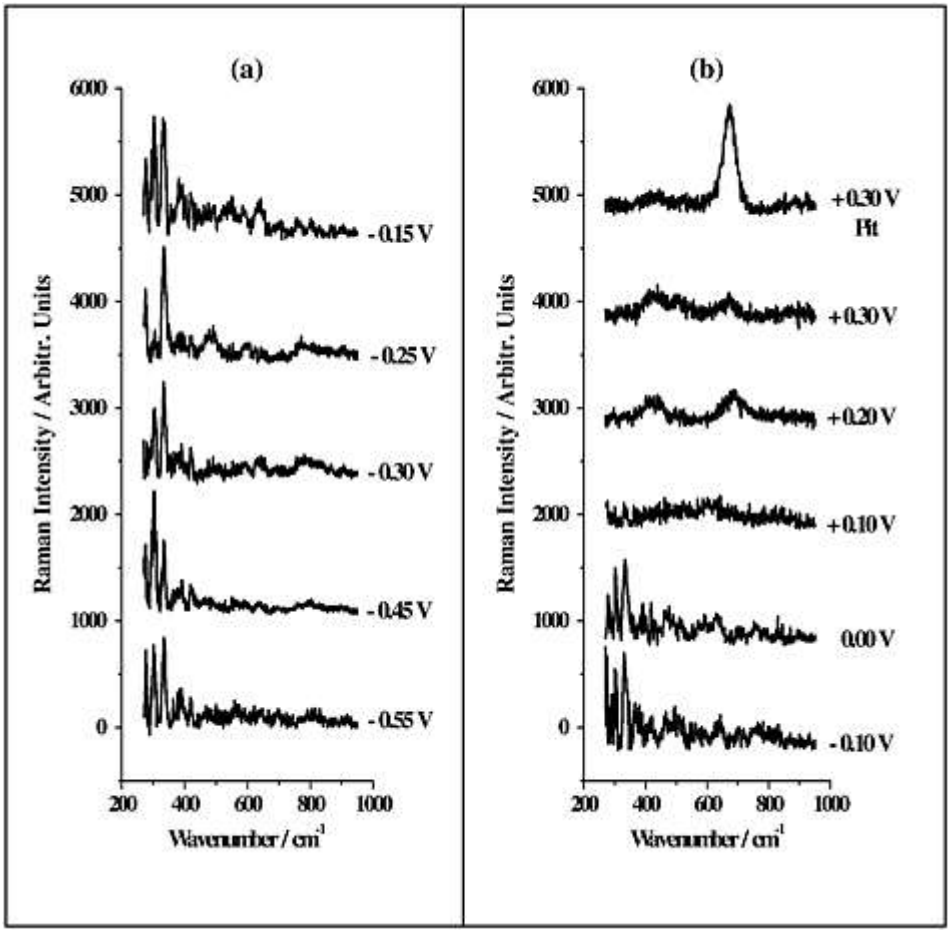

Figure 3. Raman spectra of surface recorded with preresonance enhancement while the applied potential was held for 1200 s at potentials between (a) –0.55 V and −0.15 V and (b) –0.10 V and +0.30 V, after the addition of 0.05 M NaCl to the 0.05 M NaOH solution at −0.55 V. The excitation wavelength was 636.4 nm.

When stable pitting was observed at +0.10 V, Raman spectra were recorded of various pits that were visible on the surface and of surfaces adjacent to the pits, these being shown in Fig. 4. Similar spectra were also recorded at +0.30 V, which was 0.20 V more positive than the pitting potential. These spectra are also shown in Fig. 4.

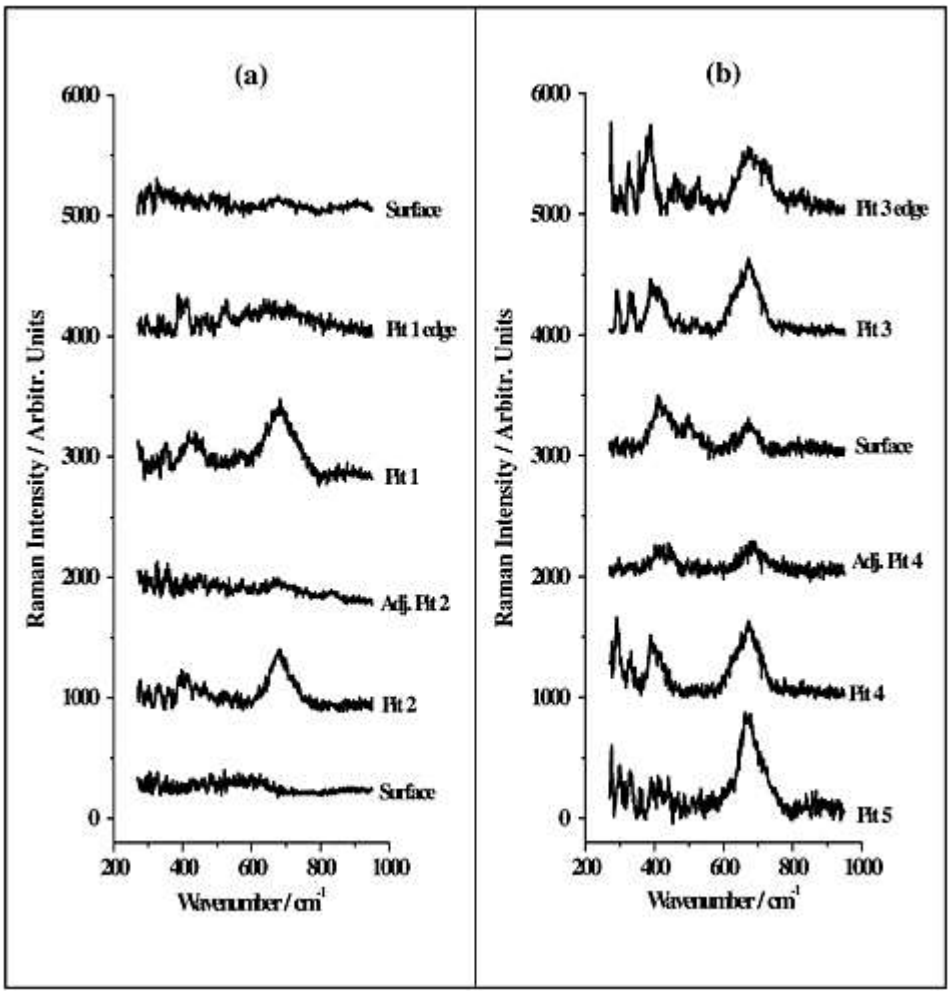

Figure 4. Raman spectra recorded *in situ* of pits and adjacent surfaces while the applied potential was held at (a) +0.10 V and (b) +0.30 V after addition of chloride ions to the 0.05 M NaOH electrolyte. The locations of the pits and their adjacent surfaces are respectively displayed in Figs 6 (Pits 1 and 2) and 7 (Pits 3, 4 and 5). The excitation wavelength was 636.4 nm.

Multivariate curve resolution with alternating least squares optimisation was used to determine the relative amounts of Green Complex, Fe_3O_4, γ-Fe_2O_3, β-FeOOH, δ-FeOOH and γ-FeOOH from the Raman spectra of Figs 3, 4(a) and (b). In all cases the compounds α-Fe_2O_3 and α-FeOOH were not present in significant amounts.

The compositional analyses shown in Fig. 5 are derived from the spectra of Fig. 4 recorded *in situ* at different potentials during anodic polarisation in the passive region. The average optimal lack of fit was 8.5%. An analysis of the composition of a pit is included in Fig. 5 for comparison purposes.

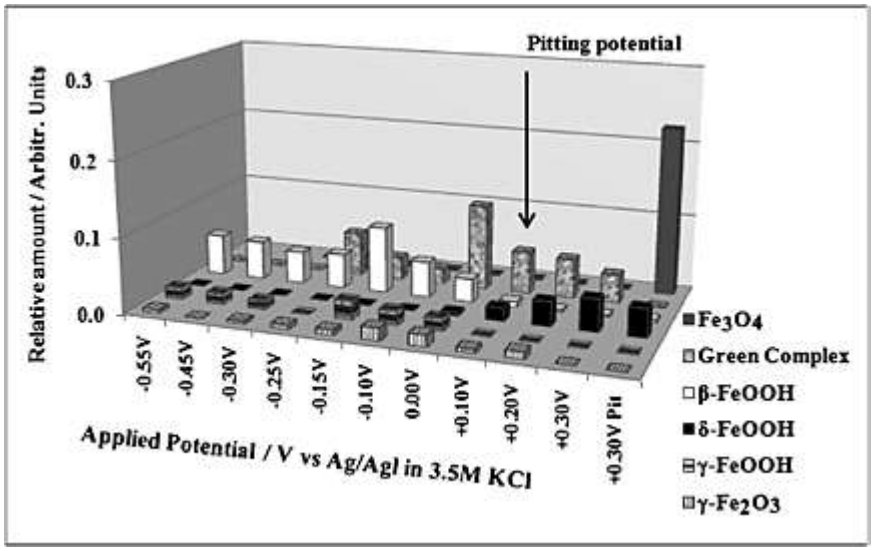

Figure 5. Relative amounts of five iron oxides determined using MCR-ALS optimisation from spectra recorded *in situ* of a 5 µm diameter area on the iron surface at different potentials in the passive region after addition of 0.05 M NaCl to the 0.05 M NaOH solution. The average optimal lack of fit was 8.5%. An analysis of the composition of a pit is included for comparison purposes.

The composition of the pit components and their adjacent surfaces corresponding to the potentials of +0.10 V and +0.30 V are shown in Figs 6 and 7, respectively, each with average optimal lack of fit values of 6.4%.

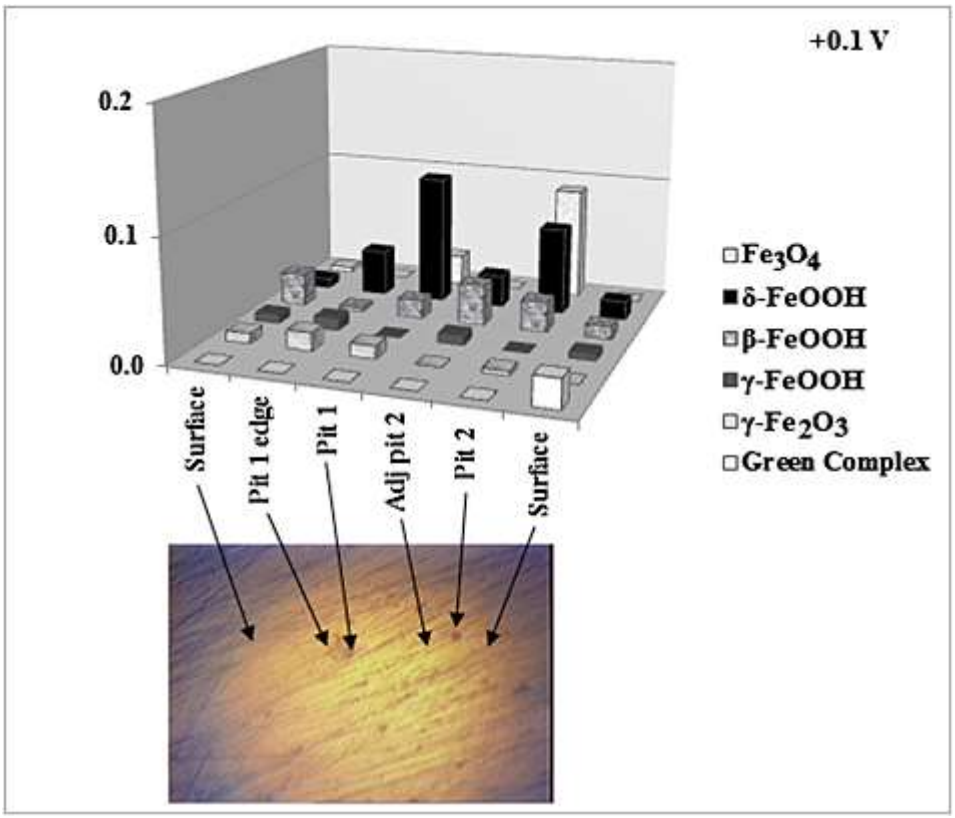

Figure 6. Relative amounts of six iron oxide components determined using MCR-ALS optimisation from spectra recorded *in situ* from pits and the surrounding areas on the iron surface during stable pitting at +0.10 V. (Photo 500 µm × 375 µm). The average optimal lack of fit was 6.4%.

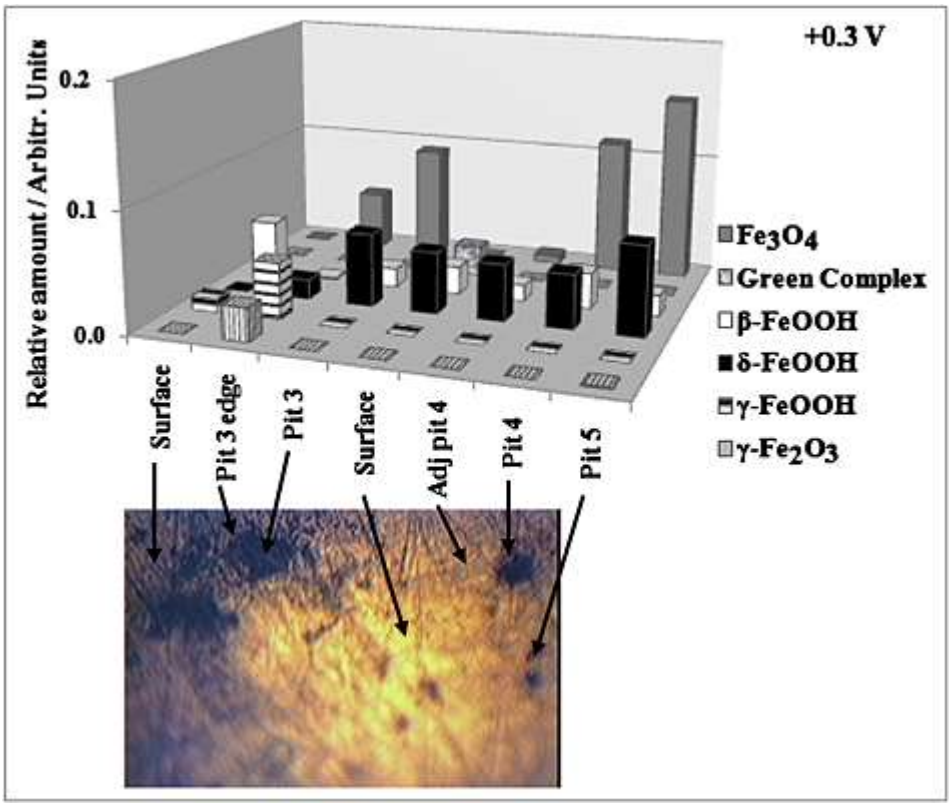

Figure 7. Relative amounts of six iron oxide components determined using MCR-ALS optimisation from spectra recorded *in situ* from pits and the surrounding areas on the iron surface during stable pitting at +0.3 V (photo 500 µm × 375 µm). The average optimal lack of fit was 6.4%.

These lack of fit values for the results of Figs 5-7 are small, considering (i) the relatively low signal-to-noise ratio of the Raman spectra of the surface areas, in spite of the preresonance enhancement and (ii) possible contributions coming from other components that were not included with the eight pure component spectra, such as $Fe(OH)_2$ and intermediate complexes, which may form during oxidation of $Fe(OH)_2$. [22] As discussed in the Experimental Section, such a residual analysis has been successfully performed in our previous work in view of a significantly larger percentage lack of fit. [27]

After removing the iron sample from the cell and allowing the surface to dry in air, Raman spectra shown in Fig. 8 were recorded of a pit that had formed and its adjacent surface. Using MCR-ALS the relative amounts of components in the pit centre were determined to be mainly Fe_3O_4 with a small amount of δ-FeOOH, while the adjacent surface contained mostly δ-FeOOH with some Fe_3O_4 and a small amount of α-Fe_2O_3.

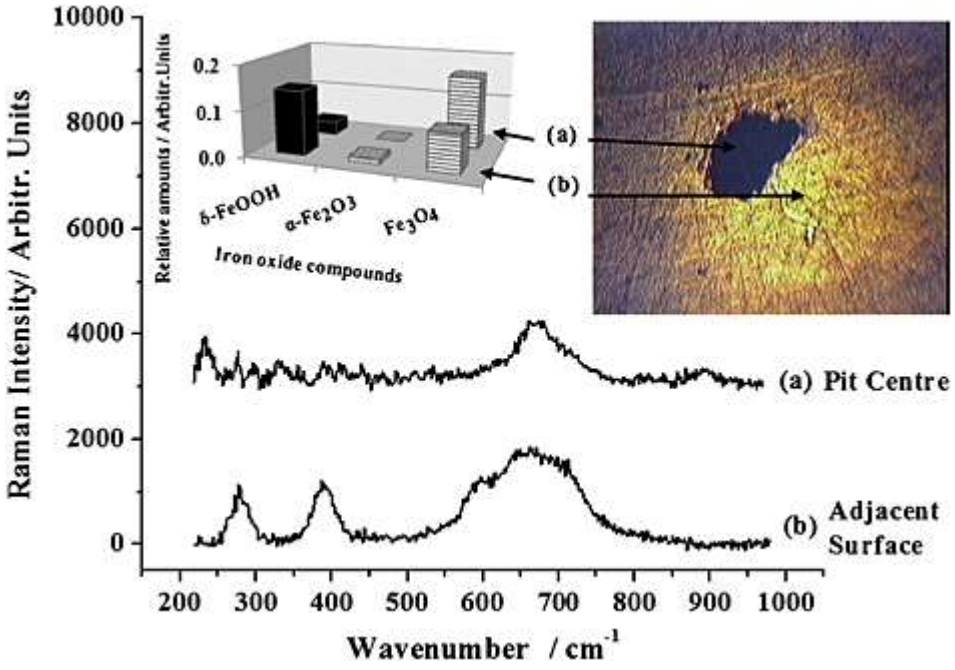

Figure 8. Raman spectra measured *ex situ*: (a) at the centre of a large pit (top right inset with a picture area of 500 µm × 375 µm) formed after being held for 1200 s at an anodic potential of +0.30 V in 0.05 M NaOH containing 0.05 M NaCl; (b) Raman spectrum of the adjacent surface measured under the same conditions as (a). The excitation wavelength was 636.4 nm. Top left inset: MCR-ALS optimisation of the spectra, showing the centre of the pit composition to be mostly Fe_3O_4 with some δ-FeOOH, and the adjacent surface mostly δ-FeOOH, with some Fe_3O_4 and a small amount of α-Fe_2O_3.

Raman spectra of the OH stretch region

Besides *in situ* spectra of the passive film in the O–H stretch region, Raman spectra were also recorded in the same region for the seven iron oxide compounds (Fe_3O_4, α-Fe_2O_3, γ-Fe_2O_3, α-FeOOH, β-FeOOH, δ-FeOOH and γ-FeOOH) at 514.5 nm and with a reduced laser power of 20 mW (0.3 mW at the sample) to avoid heating of the powders. No bands attributed to water were detected. However, four peaks at 2633, 2669, 3229 and 3479 cm^{-1} were present in the spectra; these peaks were also present in a spectrum created by light scattering from the surface of a mirror and are therefore instrumentally-induced. They were found to vary linearly in intensity with integration time.

The spectra recorded *in situ* of the O–H stretch region at the different potentials are given in Fig. 9. They include a spectrum of pure water and the instrumental peaks created with a mirror as mentioned above. The stronger instrumental peaks at 3229 and 3479 cm^{-1} overlap the spectra of the O–H mode. The weaker instrumental peaks at 2633 and 2669 cm^{-1} are indicated with asterisks and are displayed in an expanded form in the inset. The spectra were normalized such that the latter two peaks had the same intensity, the normalized spectra being used for the MCR-ALS analysis. The spectrum of the instrumental peaks at 3229 and 3479 cm^{-1} was subtracted from the raw spectrum to obtain a spectrum of pure water only. The spectra of pure water and the instrument peaks at 3229 and 3479 cm^{-1} were used as pure spectral components for the MCR-ALS optimisation of the spectra.

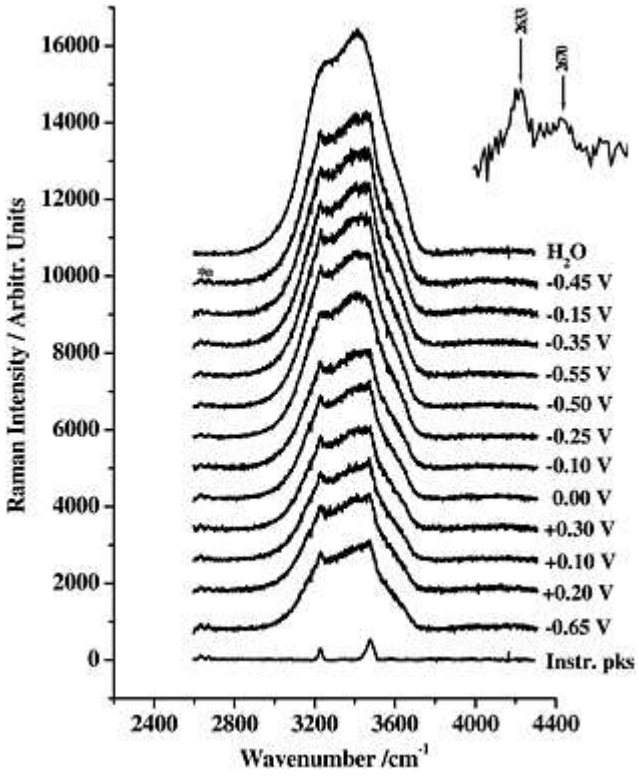

Figure 9. Raman spectra recorded *in situ* of the O–H stretch region that provide the H_2O content of the passive film at different potentials in the passive region after addition of 0.05 M NaCl to the 0.05 M NaOH solution. The two instrument peaks at 2633 and 2670 cm^{-1} (marked with asterisks) were used to normalise the Raman spectra; these are shown on an enlarged scale in the inset to the figure. The spectra of pure H_2O and the instrumental peaks at 3229 and 3479 cm^{-1} were used as pure component spectra for the MCR-ALS optimisation. The uppermost curve shows the Raman spectrum of the pure H_2O after subtraction of these instrumental peaks.

The relative amounts of water at the respective potentials determined from the MCR-ALS optimisation are plotted in Fig. 10. The average lack of fit for the optimisation was 2%.

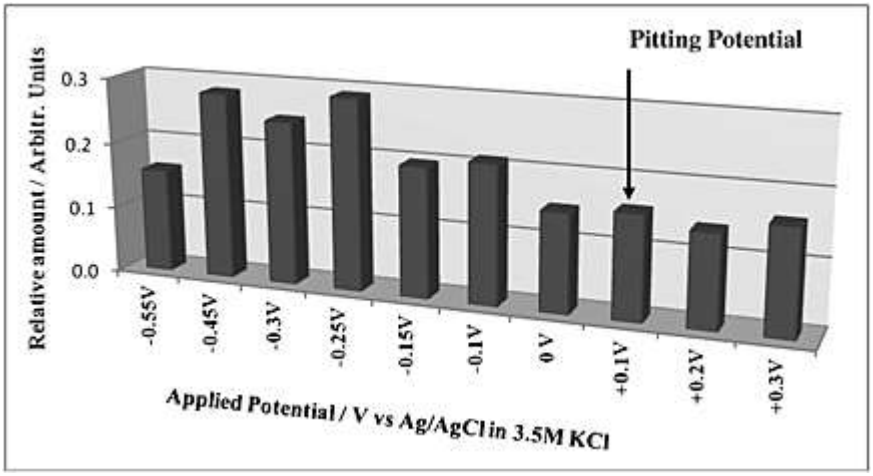

Figure 10. Relative amounts of water determined using MCR-ALS optimisation from Raman spectra recorded *in situ* of the surface in the passive region at different potentials after addition of 0.05 M NaCl. The average optimal lack of fit was 2%.

Discussion

In our previous study [27] the composition of the passive film in 0.05 M NaOH was found to be highly dependent on the applied potential. At the beginning of the passive region of the anodic potential sweep (−0.55 V) the compounds present on the surface were mainly α-FeOOH, δ-FeOOH and γ-FeOOH, which had formed as a result of oxidation during the anodic sweep. [27] As the potential was increased through the passive region, ageing of the FeOOH compounds to γ-Fe_2O_3 occurred accompanied by a decrease in the amount of water incorporated in the film. [27] In the Pourbaix diagram for iron in Fig. S2, the species expected to be stable at different pH values and potentials are determined from thermodynamic considerations. [41] At the electrolyte pH of 12.7 and in the potential region between −0.55 and 0.60 V, the species $Fe_2O_3 \cdot nH_2O$ (or 2FeOOH) are predicted and they are observed on the surface. At potentials more positive than 0 V, formation of complex aqueous FeO_4^{2-} ions is thermodynamically favourable. However, because of ageing of FeOOH compounds, a γ-Fe_2O_3 passive film is formed on the surface and this protects the iron from dissolution, which agrees with previous observations. [27]

Figure 6 shows the changes in composition of the surface film, determined by the MCR-ALS analysis, from the potential of −0.55 V at which NaCl was added to the 0.05 M NaOH solution through a series of potentials until the final potential of + 0.30 V was attained. With the addition of Cl^- ions at −0.55 V, the most significant effects in comparison with the results obtained previously are the formation of significant amounts of β-FeOOH and the absence of δ-FeOOH and α-FeOOH, these being major components in the film at this potential in the solution without Cl^- ions. [27] As the potential is increased to −0.25 V the formation of Green Complex occurs. γ-FeOOH and γ-Fe_2O_3 are present in relatively small amounts at −0.55 V and increase slightly as the potential is increased to 0 V. It is noted that a similar increase in these components was observed at these potentials in the absence of Cl^- ions. [27] It can be seen from Fig. 5 that as the pitting potential of +0.1 V is reached, significant changes occur in the composition of the film: β-FeOOH and γ-Fe_2O_3 decrease considerably and the amount of Green Complex decreases after a maximum is reached at 0 V. Simultaneously, δ-FeOOH begins to form and increases in amount with further increases in potential. In the absence of Cl^- ions the amount of δ-FeOOH was observed to decrease at potentials greater than 0 V, and at the most positive potentials of the passive region the amount of γ-Fe_2O_3 increased. [27] The addition of Cl^- ions therefore affects the way the composition of the passive film changes with increasing potential.

Another change observed in the neighbourhood of the pitting potential was a decrease in the amount of water incorporated in the passive film, as shown in Fig. 10. A similar decrease in water content was observed around the same potential without the addition of Cl^- ions, [27] which suggests that the decrease in water content in the surface film is a result of the increased anodic potential. The initial increase in the amount of water observed with increasing anodic potential followed by a decrease at higher anodic potentials agrees with observations during previous ellipsometry studies. [9, 14] In a reflectivity study [22] it was found that the higher refractive index of the passive film corresponding to higher anodic potentials is due to dehydration induced by the high anodic electric field.

However, in the present case, the migration of Cl^- ions to the anodic surface would increase under the influence of higher anodic potentials. This may also contribute to the removal of the bound water molecules by forming chloride-containing iron complexes as proposed in the hydrated polymeric model. [12]

As already described earlier in the Introduction, different roles have been suggested for the water incorporated in the passive film in the pitting of iron in the presence of Cl^- ions. In some studies the water has been described as facilitating pitting by providing paths for migration of the Cl^- ions [9] while in other studies the water incorporated in the film has been suggested to play a protective role. [5, 17] Mossbauer studies [28] inferred that the passive film has an amorphous character which is due to incorporation of water. The presence of water in the passive film was found to result in an increase in the Fe–O distance, suggesting that the H atoms introduced can lead to increased structural flexibility by forming M–OH bonds in addition to M–O bonds, which would promote a more glass-like structure for the film. [17] The amorphous nature of the film afforded by the bound water prevents Fe^{2+} from diffusing from the metal base to hydration sites at the oxide/solution interface. [5]

In a kinetic study of localized corrosion of stainless steel in the presence of Cl^- ions [18] two reactions were described to occur simultaneously at the passive film surface with Fe^{2+} ions, which have moved through the oxide film to the film/solution phase boundary and the electrolyte:

1. $Fe + 2Cl^- \rightarrow FeCl_2 + 2e^-$
2. $2Fe + 3H_2O \rightarrow Fe_2O_3 + 6H^+ + 6e^-.$

   At the same time, dissolution of the oxide can also occur:

3. $Fe_2O_3 + 6H^+ + 4Cl^- \rightarrow 2FeCl_2 + 3H_2O.$

As long as the second and third reactions occur at the same rate, the thickness of the oxide film will not change. If the second reaction occurs faster than the third, the oxide film would grow more quickly than it dissolves and the surface would repassivate; this would be encouraged by increased amounts of water and insufficient chloride concentrations. [18] On the other hand, conditions of decreased amounts of water or increased amounts of chloride ions would enable faster dissolution of the passive film, allowing the formation of stable pits. [18] This mechanism correlates well with both the hydrated polymeric and point defect models for pitting.

The mechanism is further supported by the observations in the present study of a decrease in the amount of water in the neighbourhood of the pitting potential (Fig. 10) accompanied by a change in composition of the passive film (Fig. 5). It has previously been established that more chloride is adsorbed on the surface at the pitting sites. [42] With the decrease in water observed from −0.10 V and the decrease in γ-Fe_2O_3, the dynamic equilibrium that existed up to this point between repassivation assisted by the water molecules incorporated in the film and pitting by the increased amounts of adsorbed chloride at selected sites on the surface may shift toward stable pitting.

It is noted that at the potential of 0 V, in which the amount of water decreases, there is a substantial increase in the Green Complex formation (Fig. 5). The increase in formation of this hydrated, amorphous complex at this potential is consistent with an increase in the concentration of chloride ions at the surface and occurs at the expense of water available there. The environment afforded by the Green Complex would provide conditions favourable for pitting. The δ-FeOOH formed at the pitting potential may be the oxidized product of $Fe(OH)_2$ formed from secondary reactions of dissolution products, $FeCl_2$ and NaOH. [43] Increased pitting corrosion with increasing anodic potential would result in increasing formation of δ-FeOOH. This would explain the high amount of δ-FeOOH found in the pits as shown in Figs 5-7. In a detailed study of the anodic behaviour of iron in borate buffer with added Cl^- ions, [15] pitting was found to occur at a particular stage in the formation of the passive film, which was suggested to be a transition in the development of the film when the outer phase was initially forming. This observation corresponds with the formation of δ-FeOOH at the pitting potential in the present study (Fig. 5).

The present studies indicate that stable pitting is encouraged by a combination of factors, which include high anodic potential, decrease in the amount of water in the film and decrease in the amounts of Green Complex, β-FeOOH, γ-FeOOH and γ-Fe_2O_3. Information on the events leading up to the pitting potential can be inferred from the composition of the film at the potentials just prior to pitting. Green Complex appears in the film in significant amounts at 0.0 V, just prior to the pitting potential. As mentioned earlier, the Green Complex is a hydrated, amorphous Fe_3O_4 compound, in which the iron atoms are present as both Fe^{2+} and Fe^{3+}. It has been shown that the stability of the passive film on iron is linked to the Fe^{2+} content of the passive film. [44] The decrease in β-FeOOH, γ-FeOOH and γ-Fe_2O_3 may be due to dissolution of the Fe^{3+}-containing iron oxide compounds under the influence of chloride ions, resulting in soluble Fe^{3+} and Fe^{2+} complexes, which contribute to the formation of the Green Complex. With the increased amount of Fe^{2+} already in the film, an increase in potential to 0.1 V would attract more Cl^- ions to the surface and, with further loss of β-FeOOH, γ-FeOOH and γ-Fe_2O_3, stable pitting occurs. This is accompanied by a decrease in the amount of Green Complex and the formation of δ-FeOOH on the surface. From Fig. 6 it is seen that at the pitting potential the major components of the pits are δ-FeOOH and Fe_3O_4. As the anodic potential is increased to +0.30 V (Fig. 7) the pits consisted mostly of Fe_3O_4 with smaller amounts of δ-FeOOH and β-FeOOH. The stabilisation of Fe_3O_4 in the pits is probably afforded by restricted oxygen supply in these areas because of rapid build-up of iron oxide compounds such as δ-FeOOH as an outer layer.

Ex situ spectra of the dried surface in Fig. 8 show the pit composition to be primarily Fe_3O_4 with some δ-FeOOH, while the surface adjacent to the pit indicated mainly δ-FeOOH with some Fe_3O_4 and a smaller amount of α-Fe_2O_3. However, from the *in situ* data in Figs. 5-7 neither Fe_3O_4 nor α-Fe_2O_3 was present on the surfaces adjacent to the pits; instead the composition of the surfaces consisted of various amounts of δ-FeOOH, β-FeOOH, γ-FeOOH, Green Complex and γ-Fe_2O_3.

Conclusions

Raman microscopy with preresonance enhancement has been used to examine the composition of the passive film on iron in 0.05 M NaOH (pH 12.5) in the presence of 0.05 M

NaCl under conditions of anodic polarisation. MCR-ALS analysis was used to resolve the spectra into seven individual iron oxide and oxyhydroxide compounds generally found in the passive film under these conditions, namely Fe_3O_4 (magnetite), γ-Fe_2O_3 (maghemite), α-Fe_2O_3 (hematite), α-FeOOH (goethite), β-FeOOH (akaganeite), δ-FeOOH (feroxyhyte), γ-FeOOH (lepidocrocite) and a Green Complex, which is a hydrated, amorphous magnetite compound, determined from individual spectra of these components. Hence, it was possible to determine the relative amounts of these compounds in the film. MCR-ALS analysis was also used to determine the relative amount of water from spectra recorded in the O–H stretch region.

The composition of the film is influenced by the applied anodic potential, while stable pitting occurs when a combination of conditions is reached. These are reduced water content, a change in composition of the passive film and a sufficiently high anodic potential, which results in an increased amount of Cl^- ions at the surface. Prior to stable pitting the film was composed mainly of β-FeOOH, Green Complex and smaller amounts of γ-Fe_2O_3 and γ-FeOOH. Just before the pitting potential the amounts of the Fe^{3+} containing components in the passive film decreased together with a significant increase in the amount of Green Complex, confirming previous studies linking the stability of the passive film with the Fe^{2+} content. At the pitting potential δ-FeOOH was formed and at higher potentials increased in amount, ultimately becoming a major component of the film together with significant amounts of Green Complex. The stable pits that formed were composed mainly of Fe_3O_4 with some δ-FeOOH.

The observation at the pitting potential of reduction in amount of water incorporated in the surface and change in composition confirm the mechanism of stable pitting occurring when the passive film is no longer able to maintain repassivation at the same rate as dissolution by the increased amount of locally adsorbed Cl^- ions.

The differences between the *in situ* studies within the electrolyte and *ex situ* investigations when the samples were dried show that while the compositions of the stable pits were comparable in both sets of measurements with the major components being Fe_3O_4 and δ-FeOOH, the surface compositions were substantially different. The presence of the electrolyte and *in situ* measurements are thus essential in determining the nature of the passive film and the conditions for the creation of pits.

Acknowledgement

This work was supported by the National Research Foundation under Grant number 2053306, The University of the Witwatersrand and the DST/NRF Centre of Excellence in Strong Materials.

References

[1] J. R. Galvele, in Passivity of Metals, (Eds: R. P. Frankenthal, J. Kruger), The Electrochemical Society Inc. Princeton, New Jersey, **1978**, pp. 285–327.

[2] J. Kruger, in Passivity and its breakdown on iron and iron-base alloys, (Eds: R.Staehle, H. Okada), NACE, Houston, Texas, **1976**, pp. 91–98.

[3] Y. Hisamatsu, in Passivity and its breakdown on iron and iron-base alloys, (Eds: R. Staehle, H. Okada), NACE, Houston, Texas, **1976***,* pp. 99–117.

[4] Z. Szklarska-Smialowska, Pitting Corrosion of Metals, NACE, Houston, Texas, **1986.**

[5] T. E. Pou, O. J. Murphy, V. Young, J. O'M. Bockris, J. *Electrochem. Soc.* **1984,** *131,* 1243.

[6] U. R. Evans, The Rusting of Iron: Causes and Control, Edward Arnold Ltd., London, UK, **1972.**

[7] T. Ohtsuka, J.-C. Ju, S. Ito, H. Einaga, *Corros. Sci.* **1994***, 36,* 1257.

[8] H. Konno, M. Nagayama, in Passivity of Metals, (Eds: R. P. Frankenthal, J. Kruger), The Electrochemical Society Inc., Princeton, New Jersey, **1978***,* pp. 585–606.

[9] T. Zakroczymski, C.-J. Fan, Z. Szklarska-Smialowska, *J. Electrochem. Soc.* **1985***, 132,* 2868.

[10] N. Sato, *Corros. Sci.* **1990***, 31,* 1.

[11] W. E. O'Grady, *J. Electrochem. Soc.* **1980***, 127,* 555.

[12] J. O'M. Bockris, *Corros. Sci.* **1989***, 29,* 291.

[13] S. Matsuda, K. Sugimoto, Y. Sawada, in Passivity of Metals, (Eds: R. P. Frankenthal, J. Kruger), The Electrochemical Society Inc., Princeton, New Jersey, **1978***,* pp. 699–713.

[14] N. Sato, *J. Electrochem. Soc.* **1982,** *129,* 260.

[15] J. A. Bardwell, B. MacDougall, *J. Electrochem. Soc.* **1988***, 135,* 2157.

[16]G.Okamoto, T.Shibata, in Passivity of Metals, (Eds: R. P. Frankenthal, J. Kruger), The Electrochemical Society Inc., Princeton, New Jersey **1978***,* pp. 646–667.

[17] J. Kruger*, Corros. Sci.* **1989***, 29,* 149.

[18] J. Tousek*, Corros. Sci.* **1978***, 18,* 53.

[19] Z. Q. Huang, J. L. Ord, *J. Electrochem. Soc.* **1985***, 132, 2*4.

[20] L. J. Andersson, L. J. Ojefors, *J. Electrochem. Soc.* **1976***, 123,* 824.

[21] M. Cohen, in Passivity of Metals, (Eds: R. P. Frankenthal, J. Kruger), The Electrochemical Society Inc., Princeton, New Jersey, **1978***,* pp. 521–545.

[22] T. Misawa, K. Hashimoto, S. Shimodaira, *Corros. Sci***. 1974***, 14,* 131.

[23] A. Hugot Le-Goff, S. Joiret, N. Boucherit*, Corros. Sci.* **1991***, 32,* 497.

[24] V. Rives, M. A. Ulibarri, *Coord. Chem. Rev.* **1999***, 181,* 61.

[25] V. Jovancicevic, R. C. Kainthla, Z. Tang, B. Yang, J. O'M. Bockris, *Langmuir* **1987***, 3,* 388.

[26] R. W. Revie, J. O'M. Bockris, B. G. Baker*, Surf. Sci.* **1975***, 52,* 664.

[27] M. K. Nieuwoudt, J. D. Comins, I. Cukrowski*, J. Raman Spectrosc.* **2011***, 42,* 1353.

[28] T. Misawa, K. Hashimoto, S. Shimodaira, *J. Inorg. Nucl. Chem.* **1973***, 35,* 4167.

[29] C. Gabrielli, S. Joiret, M. Keddam, N. Portail, P. Rousseau, V. Vivier, *J. Electrochem. Soc.* **2006***, 153,* B68.

[30] N. Boucherit, A. Hugot Le-Goff, S. Joiret*, Corrosion* **1992***, 48,* 569.

[31] N. Boucherit, A. Hugot-Le Goff, *Farad. Discuss.* **1982***, 94,* 137.

[32] P. Refait, M.Abdelmoula, J.-M. R. Genin, *Corros. Sci.* **1988***, 40,* 1547.

[33] L. Rongguang, R. Srinivasan, L. Spicer, B. H. Davis, *Colloids Surf. A Physicochem. Eng. Aspects* **1996***, 113,* 97.

[34] J.-M. R. Genin, P. H. Bauer, A. A. Olowe, D. Rezel, *Hyperfine Interact.* **1986,** *29,* 1355.

[35] P. Refait, J.-M. R. Genin, *Corros. Sci.* **1993***, 34,* 797.

[36] M. K. Nieuwoudt, J. D. Comins, I. Cukrowski, *J. Raman Spectrosc.* **2011***, 42,* 1335.

[37] S. Simard, M. Odziemkowski, D. E. Irish, L. Brossard, H. Menard, *J. Appl. Electrochem.* **2001,** *31,* 913.

[38] I. R. McGill, B. McEnaney, D. C. Smith, *Nature* **1976***, 259,* 2001.

[39] M. Pascale, L. Bonin, W. Jedral, M. S. Odziemkowski, R. W. Gillham, *Corros. Sci.* **2000***, 42,* 1921.

[40] J. Jaumot, R.Gargallo, A. de Juan, R. Tauler*, Chemometr. Intell. Lab. Syst.* **2005***, 76,* 101.

[41] M. Pourbaix, Atlas of Electrochemical Equilibria in Aqueous Solutions, 2nd English Edition, Pergamon Press, Oxford, UK, **1974**.

[42] C.-J. Lin, R.-G. Du, T. Nguyen*, Corrosion* **2000***, 56,* 41.

[43] H. S. Isaacs, *Corros. Sci.* **1989**, *29*, 313.

[44] W. S. Li, J. L. Luo, *Int. J. Electrochem. Sci.* **2007**, *2*, 627.

Supporting information

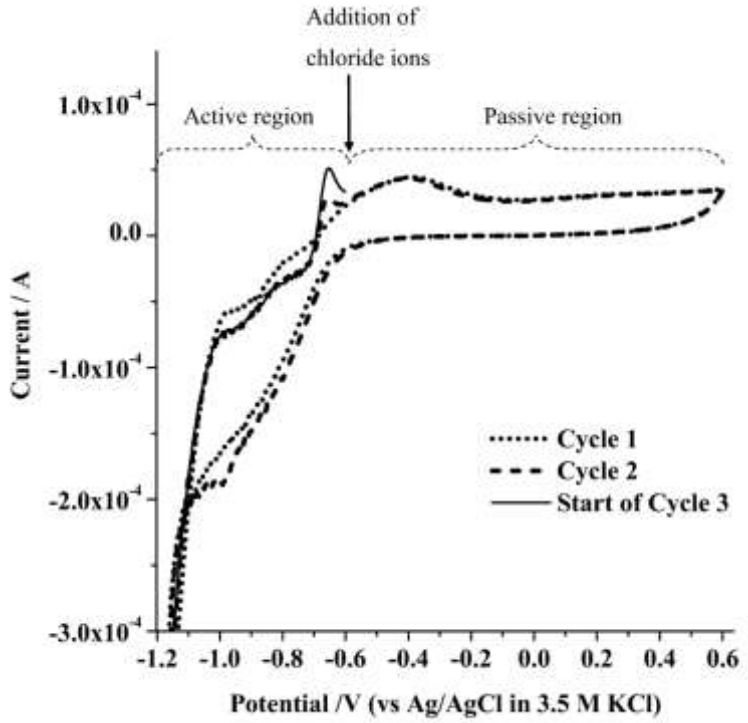

Supporting information 1

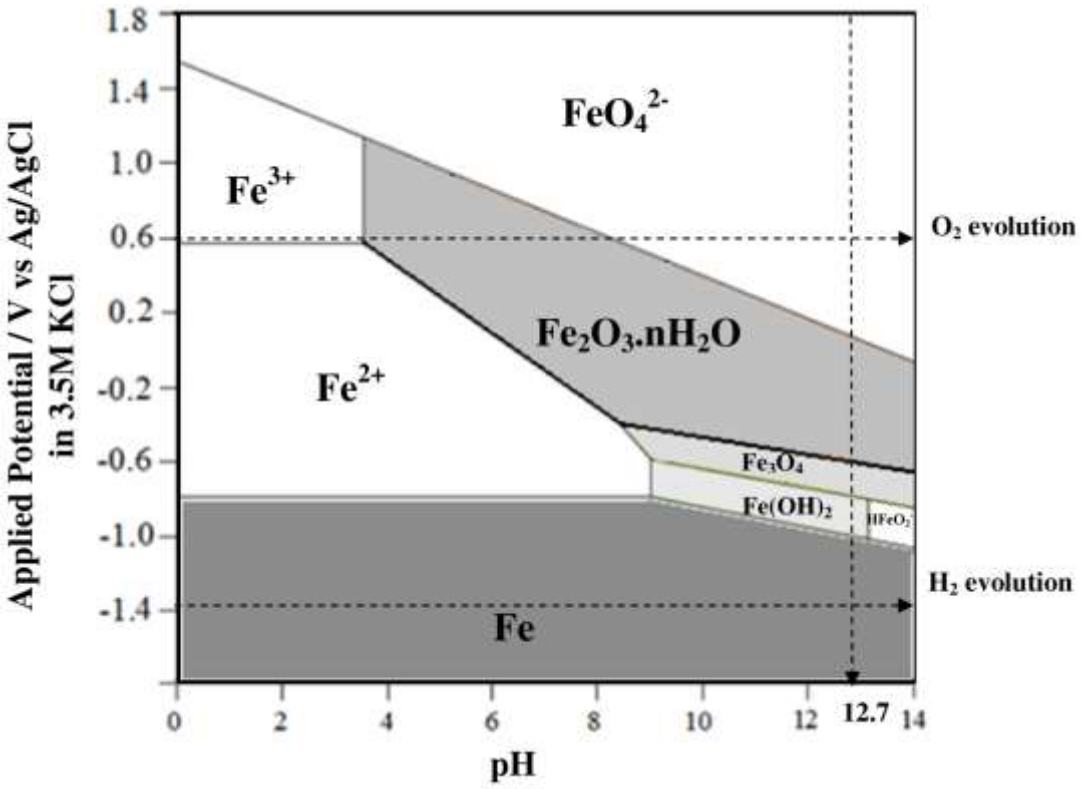

Supporting information 2